crystals

MDPI

Article

Laser Cladding of $Al_{0.5}CoCrCuFeNiSi$ High Entropy Alloy Coating without and with Yttria Addition on H13 Steel

Jingda Liu [1,2], Yuxin Guan [1,2], Xuechen Xia [1,2], Pai Peng [1,2], Qifeng Ding [1,2] and Xiaotao Liu [1,2,*]

[1] The Key Laboratory of Electromagnetic Processing of Materials, Ministry of Education, Northeastern University, Shenyang 110819, Liaoning, China; ljd18540171889@163.com (J.L.); gyx1430847737@163.com (Y.G.); 13840503068@163.com (X.X.); pengpai8111@163.com (P.P.); d893723453@163.com (Q.D.)

[2] School of Materials Science and Engineering, Northeastern University, Shenyang 110004, Liaoning, China

* Correspondence: liuxt@epm.neu.edu.cn; Tel.: +86-24-8368-9249

Received: 24 February 2020; Accepted: 9 April 2020; Published: 20 April 2020

Abstract: $Al_{0.5}CoCrCuFeNiSi$ high entropy alloy coating without and with a 1 wt.% Y_2O_3 addition was fabricated by laser cladding technique on H13 substrate. The results showed that the laser cladding coatings without and with Y_2O_3 addition consist of a mixture of body centered cubic (BCC) dendrites and face centered cubic (FCC) interdendrites. With the addition of Y_2O_3, the peaks of BCC dendrites in the coating shifted to leftwards, which is caused by the distortion of lattice due to the dissolution of Y with larger atomic radius. There exist cracks and porosities in the coating without Y_2O_3 addition. With Y_2O_3 addition, the cracks and porosities in the laser cladding coating were inhibited greatly. In addition, the microstructure of the coating with Y_2O_3 addition was refined due to the improving of the ratio of nucleation. The enhancement of properties, such as hardness, wear resistance and corrosion resistance, of the coating with Y_2O_3 addition came from the inhibition of cracks and porosities and the refinement of microstructure.

Keywords: high entropy alloys; laser cladding; hardness; wear resistance; corrosion resistance

1. Introduction

In the service of man, wear and corrosion usually initiate from the surface of engineering materials. Modifying the surface of existing materials to enhance their surface properties while not affecting the properties in the sub-surface region is more economical than fabricating the bulk materials. Various surface treatment techniques, such as laser cladding, plasma spraying process, friction stir cladding, physical vapor deposition and chemical vapor deposition, have been developed over the years [1–5]. Among these approaches, laser cladding has attracted a high level of interest of the scientific community due to its distinct advantages including faster processing rates, better control of coating thickness, minimal dilution, ease of equipment availability, maintainability and metallurgical substrate/coating bonding [6]. It has been considered as an effective and sustainable remanufacturing technique to fabricate surface coatings which permits localized processing of the difficult-to-access regions and complex structures by inducing minimal thermal distortion [7].

High entropy alloys (HEAs) are an emerging class of alloys which includes at least four or five principal elements in equimolar or close-to-equimolar ratios [8]. Multi-principal elements give rise to high configurational entropy and thus the formation of randomized solid solution phases in HEAs instead of complex intermetallic compounds as expected in traditional alloys system [9,10]. Due to their simple solid solution structure, HEAs possess an outstanding combination of strength and ductility and excellent surface properties including hardness, wear resistance, oxidation and corrosion resistance,

which make them suitable candidates for hard-facing applications [11,12]. Currently, encouraging researches on the manufacture of HEAs coating on the traditional materials have been reported [13–17].

Rare earth elements (REEs) or their oxides have been successfully employed to tailor the quality and properties of various traditional bulk materials and coatings due to their excellent physicochemical properties such as unique shell structure, outstanding chemical activity and larger ionic radii. Various studies undertaken have concluded that the absorption of REEs in the cladding materials system can potentially reduce the dilution rate, improve coating toughness, reduce cracking tendency, enhance corrosion resistance and augment bioactivity of bioceramic reimplants [18–22]. Inspired from the development of oxide dispersion strengthening (ODS) alloys, oxide particles, which act as effective pinning for grain boundaries and dislocations, were introduced into HEAs to improve their mechanical properties [23–26]. In addition, the reactive RE elements Y and Hf were doped into AlCoCrFeNi HEA by ingot metallurgy, which resulted in superior oxidation performance due to the beneficial REs-effects on the fast establishment of exclusive α-Al_2O_3 scale in early oxidation stage [27]. However, investigations on the effect of REEs or their oxides in augmenting the HEA coatings by laser cladding is still very limited.

In this paper, laser cladding technique had been used to manufacture $Al_{0.5}$CoCrCuFeNiSi HEA coatings without and with Y_2O_3 addition on H13 steel substrate. The microstructure and phase assemblage, microhardness, tribological and electrochemical properties of the HEA coatings without and with Y_2O_3 addition were investigated so as to provide an experimental basis to expand more promising application fields of both HEAs and REEs.

2. Materials and Methods

The H13 steel plate with dimensions of 40 × 40 × 10 mm^3 was used as the substrate material. The HEA $Al_{0.5}$CoCrCuFeNiSi coatings without and with 1 wt.% Y_2O_3 addition were fabricated on the substrate by laser cladding technique using elemental powders of Al, Co, Cr, Cu, Fe, Ni, Si and commercial Y_2O_3 powders with purity higher than 99.9%. Hereafter, for convenience, the HEA coatings without and with Y_2O_3 addition were denoted as HEAY0 and HEAY1, respectively. The size of the elemental powders is about 48 μm and that of the Y_2O_3 powder is in the range of 0.05–5 μm. Before laser cladding, the substrate was polished to obtain uniform roughness of ~0.2 μm and then ultrasonic-cleaned in acetone. The powders with the nominal chemical composition were mixed uniformly with α-cyanaloc acrylic resin adhesive and coated on the surface of the treated substrates to make a pre-coating about 1.5 mm in thickness. After that, the substrates with the pre-placed powders were dried in air for 2 days and then ground to a thickness of 1 mm by 1000 grade silicon carbide paper in dry condition. A JHM-1GY-800 pulsed Nd:YAG laser (CHUTIAN, Wuhan, China) with a maximum power of 800 W was used to re-melt the pre-placed layer by the relative movement between the laser beam and the substrate mounted on a four-axis numerical control working table. Argon gas blowing through a 4 mm diameter jet coaxial with the laser beam was used to shield the melt pool from oxidation and protect the laser optics from fumes and spattered particles. The experimental parameters including current, scanning speed, defocus and overlapping between tracks were optimized as 135 A, 200 mm/min, −45 mm and 45%, respectively.

An X Pertpro X-ray diffraction (XRD, PANalytical B. V., Almelo, the Netherlands) was used for the identification of the crystal structure of the laser cladding coatings without and with Y_2O_3 addition. The scanning was performed at a 2θ scan ranging from 20° to 100° at a speed of 2°/min and the typical radiation condition was 30 kV and 20 mA with a copper target. The microhardness from the laser cladding track regions to the substrate were measured using a 402MVD Vickers hardness tester (Yigong, Shanghai, China) under a load of 50 g with a dwell time of 10 s. The adhesive wear behavior of both the substrate and the laser cladding coatings were tested under dry sliding conditions at 500 °C using a MT-2000 pin-on-disk tribometer (Zhengli, Hebei, China) with a load of 100 N after 4000 rotations. The microstructure of the laser cladding coatings and the morphologies of the worn surfaces were examined using a SSX-550 scanning electron microscopy (SEM, Shimadzu, Kyoto, Japan) and the

chemical compositions were determined by energy dispersive spectrometer (EDS) equipped with SEM. The microstructure observations and the EDS analysis were performed on the cross sections of the laser cladding coatings which were cut perpendicular to the laser tracks.

The electrochemical properties of specimen were measured by the CHI650D electrochemical analyzer (CH Instruments, Shanghai, China). The specimens after slightly polishing with silicon carbide paper (2500 grit) were decreased in benzene, cleaned ultrasonically and washed with distilled water prior to electrochemical tests. To study the corrosion behaviors of the substrate and the laser cladding coatings, a three-electrode cell arrangement was used for the electrochemical measurements with a saturated calomel electrode (SCE) as the reference electrode, a platinum plate as the auxiliary electrode and specimen as the working electrode with an exposed area of 1 cm^2 in 3.5 vol.% NaCl solution at 23 ± 1 °C open to air and repeated several times to ensure the reproducibility of the data. Potentiodynamic polarization scan started from −0.65 V to 0.55 V with a sweep rate of 1 mVs^{-1} and the Tafel region was analyzed by using DC105 software (Shanghai, China).

3. Results

3.1. Microstructure and XRD Analysis

The XRD patterns of $Al_{0.5}CoCrCuFeNiSi$ HEA coatings without and with Y_2O_3 addition are shown in Figure 1. The Bragg peaks in the XRD pattern of the coating can be indexed to a mixture of body centered cubic (body centered cubic) and face centered cubic (FCC) simple solid solution structures in the laser cladding HEA coatings both without and with Y_2O_3 addition. The much stronger peak intensity of BCC phase suggests that the BCC structure is a dominative phase in the coatings. There are no peaks for Y_2O_3 or new generated phase detected in the XRD patterns of the laser cladding HEA coating with Y_2O_3 addition, which may be due to the small addition of Y_2O_3 which is beyond the detection limit of XRD. The average full width of half maximum (FWHM) of BCC diffraction peaks are 0.42 and 0.44 for the laser cladding coatings without and with Y_2O_3 addition, respectively. The average full width at half maximum (FWHM) of the BCC diffraction peaks increase with the addition of Y_2O_3 indicating that the BCC grains were refined after adding Y_2O_3. Figure 1b shows an enlarged picture of the main peak of BCC phase in the laser cladding HEA coating without and with Y_2O_3 addition. It is also shown that the peaks of the BCC phases shifted leftwards with the addition of Y_2O_3, indicating that the lattice parameter of the BCC phases increases. By linearity extrapolation method, the lattice constants of the BCC phase were 2.834 Å and 2.856 Å for the laser cladding coatings without and with Y_2O_3 addition, respectively.

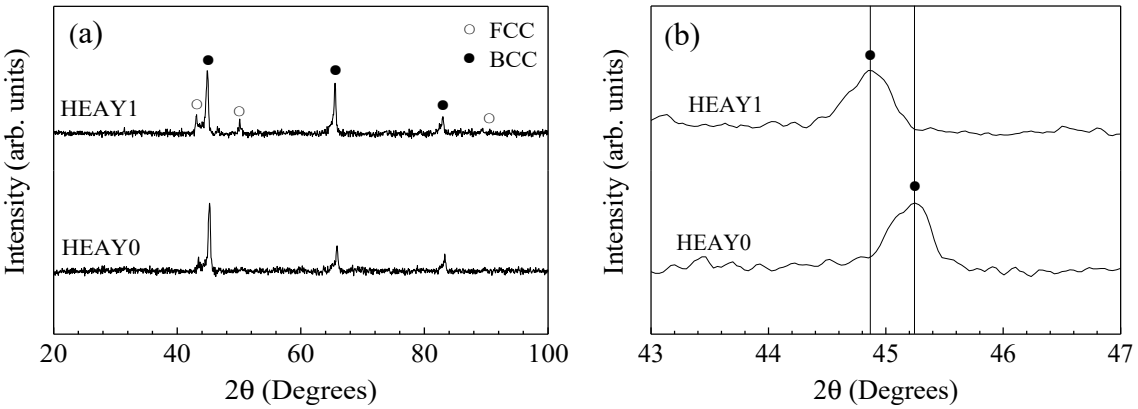

Figure 1. X-ray diffraction (XRD) diffraction patterns for the laser cladding high entropy alloy (HEA) coatings without and with Y_2O_3 addition (**a**); An enlarged picture of the main peak of BCC phase (**b**).

Figure 2 shows the cross-sectional microstructure of the laser cladding HEA coatings without (Figure 2a–c) and with Y_2O_3 addition (Figure 2d–f). For the laser cladding HEA coating without Y_2O_3,

transverse cracks have been observed, which are perpendicular to the scanning direction (perpendicular to the paper) and stop at the coating/substrate interface. Furthermore, the cracks expand with radial shape. On the contrary, with the addition of 1 wt.% Y_2O_3, the cracks in the laser cladding HEA coating were inhibited, as shown in Figure 2d. Figure 2b,c represent the microstructure of the local amplification of area A and B as indicated by the squares in Figure 2a. Figure 2e,f represent of the local amplification of area C and D as indicated by the squares in Figure 2d. The back scattered electron (BSE) images shows that the laser cladding coating both without and with Y_2O_3 addition have a typical dendrite microstructure after solidification, i.e., a large amount of dendrite phases (dark contrast) with BCC structure and a small quantity of interdendrite phases (bright contrast) with FCC structure. The EDS analysis as shown in Figure 3 indicates that there is Cu element segregation in the interdendrite region, and other elements are rich in the dendrite region, which is consistent with our previous report [28]. For the laser cladding HEA coating without Y_2O_3 addition, significant porosities are observed and the dendrite near the coating/substrate interface is vertical, directional and epitaxial to the bonding interface. However, with the addition of Y_2O_3, both the number density and the size of the porosities in the coating were greatly reduced and the solidification microstructure near coating/substrate interface is no longer epitaxial and directional to the bonding interface.

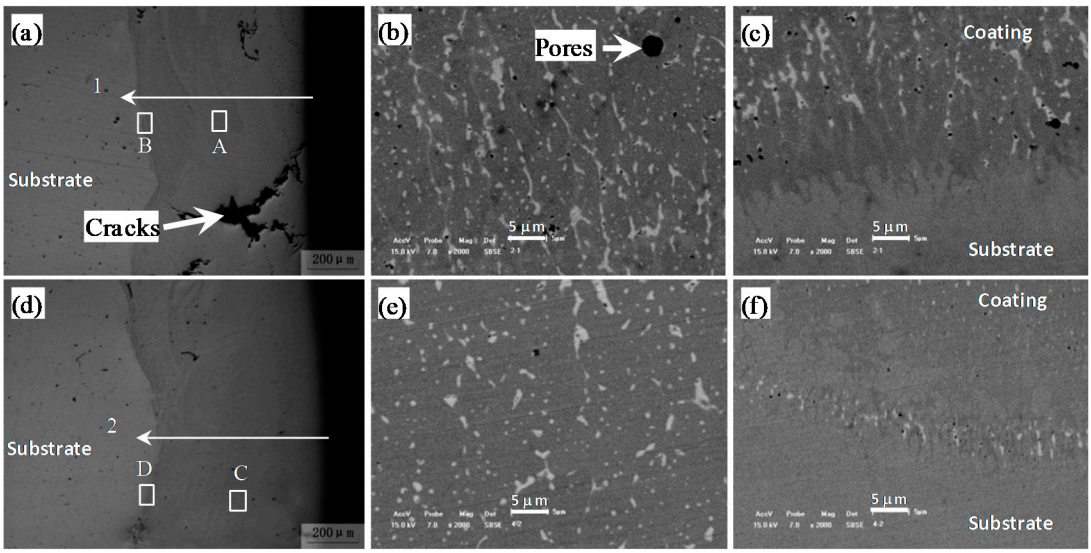

Figure 2. Cross-sectional microstructure for the laser cladding HEA coatings without and with Y_2O_3 addition. (**a**) Cross section of coating without Y_2O_3; (**b**) high magnification image from the middle of the coating as indicated by square A in Figure 2a; (**c**) high magnification image close to the interface as indicated by square B in Figure 2a; (**d**) cross section of coating with Y_2O_3 addition; (**e**) high magnification image from the middle of the coating as indicated by square C in Figure 2d; (**f**) high magnification image close to the interface as indicated by square D in Figure 2d. Lines in (a) and (d) denote the linescan along which quantitative energy dispersive spectrometer (EDS) line analysis (Figure 3) was performed.

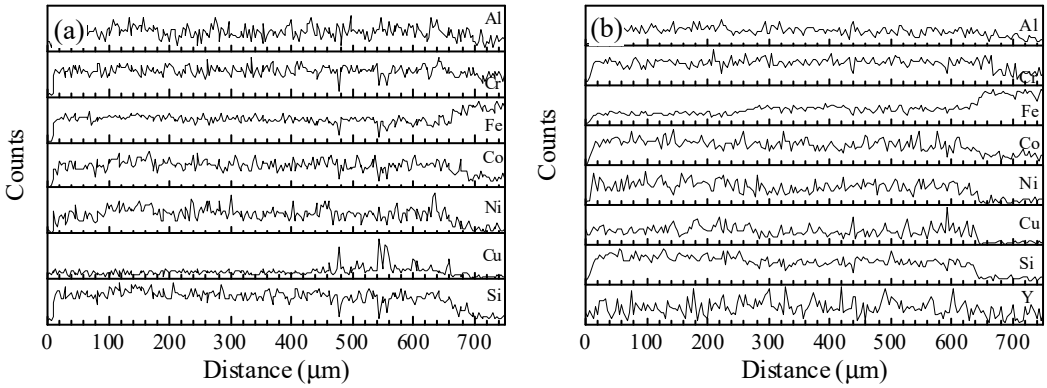

Figure 3. Quantitative EDS line analysis over the thickness of the laser cladding HEA coatings without and with Y_2O_3 as indicated by line 1 and 2 in Figures 2a and 2d, respectively. (**a**) Without Y_2O_3; (**b**) with Y_2O_3.

3.2. Microhardness and Wear Resistance

Figure 4 presents the microhardness variations ranging from the laser cladding coatings without and with Y_2O_3 addition to the substrate. It is apparent that both of the laser cladding coatings show higher hardness than the H13 steel substrate. The average hardness, 491 HV and 599 HV, of the laser cladding coatings without and with Y_2O_3 addition, respectively, are 2.43 and 2.97 times that, 202 HV, of the bare substrate. Furthermore, compared to the cladding coating without Y_2O_3 addition, the hardness of the cladding coating with Y_2O_3 addition increased and the hardness distribution throughout the coating in depth was much more uniform. The tribological performances of the laser cladding coatings were evaluated by subjecting them to adhesive wear at 500 °C and compared to that of the bare substrate tested at identical conditions. The wear resistance of the laser cladding coatings without and with Y_2O_3 addition, as well as that of the bare substrate, are shown in Figure 5. The wear resistance, 0.24 km/mm^3 and 0.47 km/mm^3, for the laser cladding coating without and with Y_2O_3 addition, respectively, are 160% and 209% that, 0.15 km/mm^3, of the bare substrate. The insert in Figure 5 represents the friction coefficients of the substrate and the laser cladding coatings. The friction coefficients of the laser cladding coatings are lower than that of the substrate, also corroborating the wear behavior improvement.

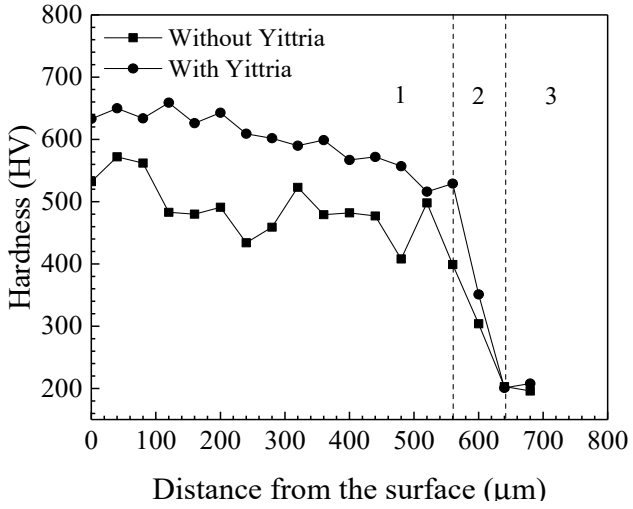

Figure 4. Microhardness distribution ranging from laser cladding coatings to substrate. 1, 2 and 3 denote the laser cladding coating, transition zone and substrate, respectively.

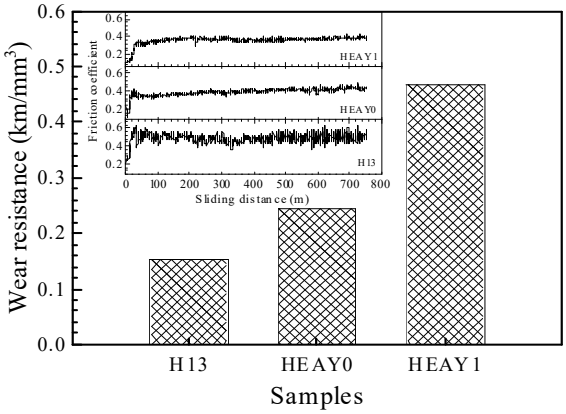

Figure 5. Weight loss and coefficient of friction for H13 substrate and laser cladding coatings without and with Y_2O_3 addition.

Figure 6 shows the morphologies of the worn surfaces of the bare substrate and the laser cladding coatings without and with Y_2O_3 addition. Distinct differences in the worn surface morphologies are seen. For the bare substrate (Figure 6a), the worn surface was grooved and significant ductile deformation along the groove can be seen, and cracks are observed on the worn surface. It indicates that the adhesive wear of the bare substrate at 500 °C is predominantly of delamination wear by which the worn surface undergoes a periodic delamination fracture [29]. However, for the laser cladding coating without Y_2O_3 addition, the plastic features and grooves were inhibited greatly and the worn surfaces are much smoother with fewer shallow grooves. The worn surface of the cladding layer with Y_2O_3 is even smoother than that of the cladding coating without Y_2O_3 addition. It is indicated that the laser cladding HEA coating with Y_2O_3 addition shows the best wear resistance, followed by the laser cladding HEA coating without Y_2O_3 addition, and the bare substrate the worst.

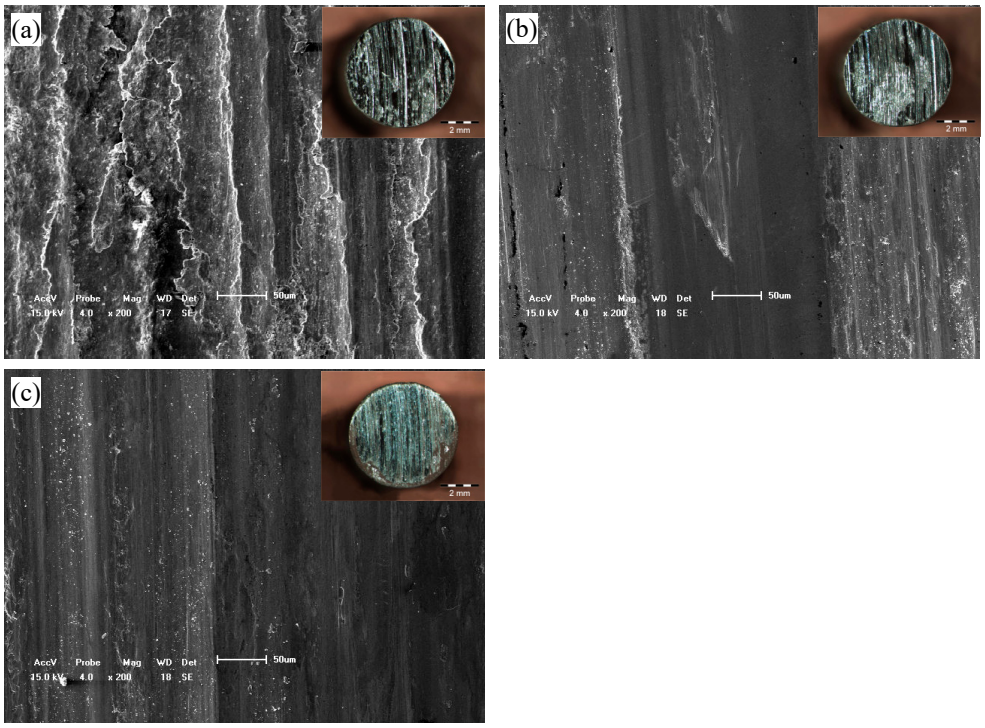

Figure 6. Morphologies of the worn surface of specimens after wear test. (**a**) The H13 substrate; (**b**) laser cladding coating without Y_2O_3 addition; (**c**) laser cladding HEA coating with Y_2O_3 addition. The insert on each image represents the overall morphology of the worn surface.

3.3. Corrosion Resistance

The polarization curves of laser cladding HEA coatings without and with Y_2O_3, as well as the bare substrate, tested in 3.5 vol.% NaCl solution under identical conditions are shown in Figure 7. Tafel curve extrapolation method was carried out to determine the electrochemical parameters including the corrosion potential (E_{corr}) and the corrosion current density (I_{corr}) which were listed in Table 1. The E_{corr} values of the laser cladding HEA coatings without and with Y_2O_3 addition are all more positive than that of the substrate, while the I_{corr} values of the laser cladding coatings are obviously lower than that of the substrate. Further, the laser cladding HEA coating with Y_2O_3 addition exhibits higher E_{corr} and lower I_{corr} compared to those of the HEA coating without Y_2O_3.

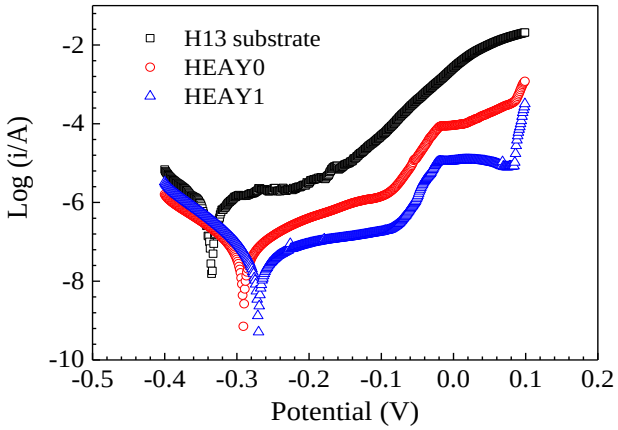

Figure 7. Potential polarization curves for H13 substrate and laser cladding coatings without and with Y_2O_3 addition.

Table 1. The corrosion potential (E_{corr}) and corrosion current density (I_{corr}) derived from the potential polarization curves.

E_{corr} or I_{corr}	H13	HEAY0	HEAY1
E_{corr} (mV)	−335	−291	−269
I_{corr} (A)	6.58×10^{-7}	3.58×10^{-8}	3.35×10^{-8}

The results of the electrochemical impedance measurements obtained for the substrate and laser cladded specimens in 3.5% NaCl solution are displayed as Nyquist plots in Figure 8. It can be seen that the Nyquist diagrams showed an unfinished semicircle arc for all the specimens. The semicircle arc represents film impedance at high frequencies and a low frequency electron transfer reaction response. The formation of such semicircle arc is attributed to the charge transfer process at the electrode/electrolyte interface, related to changes in the passive oxide property and their chemical composition. Differences were observed in all the impedance spectra between the laser cladded specimens and the substrate. For the substrates, the semicircle radius was smaller than the laser cladded coatings. The increase in semicircle radius for the laser cladded coating indicated an increase in the passive film stability and corrosion resistance. It is indicated that the HEA coating with Y_2O_3 addition provides the best corrosion resistance, followed by HEA coating without Y_2O_3 and the bare substrate the worst.

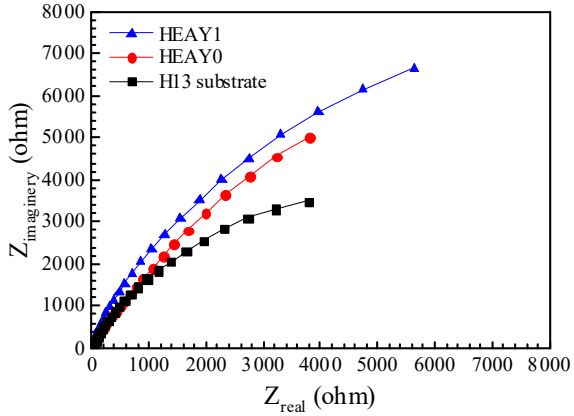

Figure 8. The electrochemical impedance measurements as Nyquist plots obtained for the substrate and laser cladded specimens in 3.5% NaCl solution.

4. Discussion

For laser cladding of HEA coating, thermal entropy contribution adds to the configurational entropy making conditions suitable for solid solution phases formation at high temperature and rapid quenching ensures retention of the solid solution phase at room temperature. As indicated by the XRD and microstructural analysis, the $Al_{0.5}$CoCrCuFeNiSi HEA coatings consist of BCC structured dendrites and minor FCC structured interdendrites. In this HEA, the mixing enthalpy of Cu–Co, Cu–Cr, Cu–Fe atomic pairs have positive values. As for Si, though the mixing enthalpy between Si and Cu, −19 kJ/mol, is negative, it is still a relatively positive value among the mixing enthalpies between Si and the other components. Thus, the Cu atoms were rejected segregate to the interdendrites during solidification due to its relative positive mixing enthalpy values with the other components. Surface cracks with deep penetration into the cladding for the HEA coating without Y_2O_3 addition, as shown in Figure 2a, is due to the strong convective flow and surface tension gradient in the melt pool and the rapid solidification leading to the existence of remnant stress in the coating after laser treatment [20]. Porosities observed in the HEA cladding coating without Y_2O_3 addition could be explained by the gas trapping due to large fluid viscosity induced by material particles in the melt pool and the encapsulated bubbles generated during laser cladding process [30].

Rare earth elements possess particular atomic structure and excellent chemical activity. With the addition of Y_2O_3 into cladding powders, the Y_2O_3 can be partially decomposed in the molten pool under the irradiation of high-energy laser beam and therefore the solidification pattern and surface tension gradients will be modified [30]. The decomposed Y could act as surfactant which reduces the surface tension and interfacical energy and thus the work for forming nuclei with critical size improving the ratio of nucleation and refining the grains. Y_2O_3 could also be considered as nuclei in the melting pool and refine the microstructure due to its higher melting temperature. Due to its excellent chemical activity, the decomposed Y can react with elements such as oxygen, sulfur, nitrogen and so on, forming stable and high-melting-point compounds which will float on the melt and be cleaned off the clad layer as molten slag during laser cladding process. The changes of solidification pattern and surface tension gradients, the microstructural refinement and the purification of the coating due to the addition of Y_2O_3 will lower cracking tendency during solidification of the HEA coating.

Compared to the substrate, the improved mechanical properties of the laser cladding HEA coating without Y_2O_3 addition are attributed to the presence of BCC structured simple solid solution phase, as indicated by the XRD analysis, which are much harder and stronger due to its intrinsic structural characteristics. The increase in hardness and wear resistance of the laser cladding HEA coating with Y_2O_3 addition come from the refining effect of Y_2O_3 on the microstructure and solution hardening mechanism. The addition of Y_2O_3 into HEA coating leads to the refinement of the microstructure, which improves the hardness and strength of the cladding coating. For the solution hardening mechanism

factor, the dissolution of Y atoms with larger radius (1.80 Å) into the BCC crystal lattice causes severe lattice distortion and thus increase the local elastic stress field which interacts with the stress field of dislocations and hinders the movements of dislocations causing strengthening. The uniform hardness distribution along depth in the laser cladding HEA coating with Y_2O_3 addition came from the elimination of porosities and cracks and the refinement of the microstructure. The enhancement of wear resistance for laser cladding coatings is due to the higher hardness which can resist the plastic deformation, particularly the laser cladding coating with Y_2O_3 addition.

In corrosion tests, the microstructures of coating played a dominate role. In the coating without Y_2O_3, cracks and porosities were observed, as indicated in Figure 2a,b. The cracks could act as liquid channels and the corrosive medium might flow to the coating/substrate interface from the surface coating. Consequently, the substrate exposed to the electrolyte would be attacked by crevice corrosion. Due to the existence of porosities, the electrolyte could be trapped and stagnated in the pores causing the dissolution of the peripheral region, which results in the interconnection of the isolated pores forming a liquid channel. Either crevice corrosion, similar to that caused by cracks, or localized corrosion might occur depending on the width of the channels. With the addition of Y_2O_3 in the coating material, the cracks and porosities of coating were reduced greatly or even eliminated. Furthermore, due to the refining and purifying effect of Y_2O_3, the active center with different potential, which result in the formation of microcells and electrochemical corrosion, will be reduced or even eliminated and thus the surface potential will tend to be uniform.

5. Conclusions

1. The laser cladding HEA coating without and with Y_2O_3 addition consisted of a mixture of BCC structure dendrites and FCC interdendrites. The addition of Y_2O_3 has no effects on the crystal structure but the lattice constant of the BCC dendrites increased with the addition of Y_2O_3.
2. Cracks and porosities were observed in the laser cladding coating without Y_2O_3. With the addition of Y_2O_3, the cracks and porosities were inhibited and the microstructure was refined due to the improving of the ratio of nucleation.
3. The properties enhancement of the laser cladding coating without Y_2O_3 addition is due to the intrinsic characteristic of BCC structured solid solution phase. With the addition of Y_2O_3 in the coating material, the properties were further improved due to the inhibitation of cracks and porosities and the refining of the microstructure.

Author Contributions: Conceptualization, X.L.; data curation, J.L., Y.G. and X.L.; investigation, J.L., Y.G., X.X., P.P. and Q.D.; methodology, J.L., X.X., X.L. and Y.G.; supervision, X.L.; writing—Original draft, J.L. and X.X.; writing—Review and editing, X.L. All authors have read and agreed to the published version of the manuscript.

Funding: This research was funded by National Training Program of Innovation and Entrepreneurship for Undergraduates (Grant number: 201910145257), the Fundamental Research Funds for the Central Universities (Project number: N182410001) and by the In-house funding from the Key Lab of EPM of NEU (Grant number: NEU-EPM-002).

Conflicts of Interest: The authors declare no conflict of interest.

References

1. Yang, J.X.; Wu, F.Y.; Bai, B.; Wang, G.S.; Yang, L.; Zhou, S.F.; Lei, J.B. Effect of Cr additions on the microstructure and corrosion resistance of Diode laser clad CuAl10 coating. *Surf. Coat. Technol.* **2020**, *381*, 125215. [CrossRef]
2. Bobzin, K.; Brogelmann, T.; Kalscheuer, C.; Welters, M. Structure, mechanical characteristics and thermal stability of high speed physical vapor deposition $(Al,Cr)_2O_3$ coatings. *Thin Solid Films* **2019**, *690*, 137529. [CrossRef]
3. Kainz, C.; Schalk, N.; Tkadletz, M.; Saringer, C.; Winkler, M.; Stark, A.; Schell, N.; Julin, J.; Czettl, C. Thermo-physical properties of coatings in the Ti(B, N) system grown by chemical vapor deposition. *Surf. Coat. Technol.* **2020**, *384*, 125318. [CrossRef]

4. Xiao, J.K.; Tan, H.; Wu, Y.Q.; Chen, J.; Zhang, C. Microstructure and wear behavior of FeCoNiCrMn high entropy alloy coating deposited by plasma spraying. *Surf. Coat. Technol.* **2020**, *385*, 125430. [CrossRef]
5. Xiong, X.M.; Yang, Y.; Li, J.G.; Li, M.M.; Peng, J.; Wen, C.; Peng, X.D. Research on the microstructure and properties of a multi-pass friction stir processed 6061Al coating for AZ31 Mg alloy. *J. Magnes. Alloys* **2019**, *7*, 696–706. [CrossRef]
6. Birger, E.M.; Moskvitin, G.V.; Polyakov, A.N.; Arkhipov, V.E. Industrial laser cladding: Current state and future. *Welding Int.* **2011**, *25*, 234–243. [CrossRef]
7. Santo, L. Laser cladding of metals: A review. *Int. J. Surf. Sci. Eng.* **2008**, *2*, 327–335. [CrossRef]
8. Zou, Y.; Maiti, S.; Steurer, W.; Spolenak, R. Size-dependent plasticity in an $Nb_{25}Mo_{25}Ta_{25}W_{25}$ refractory high entropy alloy. *Acta Mater.* **2014**, *65*, 85–97. [CrossRef]
9. Yeh, J.-W.; Chen, S.-K.; Lin, S.-J.; Gan, J.-Y.; Chin, T.-S.; Shun, T.-T.; Tsau, C.-H.; Chang, S.-Y. Nanostructured high-entropy alloys with multiple principal elements: Novel alloy design concepts and outcomes. *Adv. Eng. Mater.* **2004**, *6*, 299–303. [CrossRef]
10. Cantor, B.; Chang, I.T.H.; Knight, P.; Vincent, A.J.B. Microstructural development in equiatomic multicomponent alloys. *Mater. Sci. Eng. A* **2004**, *375–377*, 23–218. [CrossRef]
11. Tsai, M.H.; Yeh, J.W. High-entropy alloys: A critical review. *Mater. Res. Lett.* **2014**, *2*, 107–123. [CrossRef]
12. Gludovatz, B.; Hohenwarter, A.; Cantor, D.; Chang, E.H.; George, E.P.; Ritchie, R.O. A fracture resistant high-entropy alloy for cryogenic applications. *Science* **2014**, *345*, 1153–1158. [CrossRef] [PubMed]
13. Yue, T.M.; Xie, H.; Lin, X.; Yang, H.O.; Meng, G.H. Solidification behaviour in laser cladding of AlCoCrCuFeNi high-entropy alloy on magnesium substrates. *J. Alloys Compd.* **2014**, *587*, 588–593. [CrossRef]
14. Jiang, Y.Q.; Li, J.; Juan, Y.F.; Lu, Z.J.; Jia, W.L. Evolution in microstructure and corrosion behavior of $AlCoCr_xFeNi$ high-entropy alloy coatings fabricated by laser cladding. *J. Alloys Compd.* **2017**, *775*, 1–14. [CrossRef]
15. Cai, Z.B.; Wang, Y.D.; Cui, X.F.; Jin, G.; Li, Y.; Liu, Z.; Dong, M.L. Design and microstructure characterization of FeCoNiAlCu high-entropy alloy coating by plasma cladding: In comparison with thermodynamic calculation. *Surf. Coat. Technol.* **2017**, *330*, 163–169. [CrossRef]
16. Zhang, G.J.; Tian, Q.W.; Yin, K.X.; Niu, S.Q.; Wu, M.H.; Wang, W.W.; Wang, Y.N.; Huang, J.C. Effect of Fe on microstructure and properties of AlCoCrFexNi (x = 1.5, 2.5) high entropy alloy coatings prepared by laser cladding. *Intermetallics* **2020**, *119*, 106722. [CrossRef]
17. Cui, Z.Q.; Qin, Z.; Dong, P.; Mi, Y.J.; Gong, D.Q.; Li, W.G. Microstructure and corrosion properties of FeCoNiCrMn high entropy alloy coatings prepared by high speed laser cladding and ultrasonic surface mechanical rolling treatment. *Mater. Lett.* **2020**, *259*, 126769. [CrossRef]
18. Wang, K.L.; Zhang, Q.B.; Sun, M.L.; Wei, X.G. Microstructural characteristics of laser clad coatings with rare earth metal elements. *J. Mater. Process. Technol.* **2003**, *139*, 448–452. [CrossRef]
19. Li, J.; Luo, X.; Li, G.J. Effect of Y_2O_3 on the sliding wear resistance of TiB/TiC-reinforced composite coatings fabricated by laser cladding. *Wear* **2014**, *310*, 72–82. [CrossRef]
20. Wang, D.S.; Liang, E.J.; Chao, M.J.; Yuan, B. Investigation on the microstructure and cracking susceptibility of laser-clad V_2O_5/NiCrBSiC alloy coatings. *Surf. Coat. Technol.* **2008**, *202*, 1371–1378. [CrossRef]
21. Zhu, R.; Li, Z.; Li, X.; Sun, Q. Microstructure and properties of the low-power-laser clad coatings on magnesium alloy with different amount of rare earth addition. *Appl. Surf. Sci.* **2015**, *353*, 405–413. [CrossRef]
22. Li, H.C.; Wang, D.G.; Chen, C.Z.; Weng, F. Effect of CeO_2 and Y_2O_3 on microstructure, bioactivity and degradability of laser cladding CaO-SiO_2 coating on titanium alloy. *Colloids Surf. B* **2015**, *127*, 15–21. [CrossRef] [PubMed]
23. Prasad, H.; Singh, S.; Panigrahi, B.B. Mechanical activated synthesis of alumina dispersed FeNiCoCrAlMn high entropy alloy. *J. Alloys Compd.* **2017**, *692*, 720–726. [CrossRef]
24. Praveen, S.; Anupam, A.; Sirasani, T.; Murty, B.S.; Kottada, R.S. Characterization of oxide dispersed AlCoCrFe high entropy alloy synthesised by mechanical alloying and spark plasma sintering. *Trans. Indian Inst. Met.* **2013**, *66*, 269–373. [CrossRef]
25. Hadraba, H.; Chlup, Z.; Dlouhy, A.; Dobes, F.; Roupcova, P.; Vilemova, M.; Matejicek, J. Oxide dispersion strengthened CoCrFeNiMn high-entropy alloy. *Mater. Sci. Eng. A* **2017**, *689*, 252–256. [CrossRef]
26. Gwalani, B.; Pohan, R.M.; Lee, J.; Lee, B.; Banerjee, R.; Ryu, H.J.; Hong, S.H. High-entropy alloy strengthened by in situ formation of entropy-stabilized nano-dispersoids. *Sci. Rep.* **2018**, *8*, 14085. [CrossRef]

27. Lu, J.; Chen, Y.; Zhang, H.; Ni, N.; Li, L.; He, L.M.; Mu, R.D.; Zhao, X.F.; Guo, F.W. Y/Hf-doped AlCoCrFeNi high-entropy alloy with ultra oxidation and spallation resistance. *Corros. Sci.* **2020**, *166*, 108426. [CrossRef]
28. Liu, X.T.; Lei, W.B.; Ma, L.J.; Liu, J.; Liu, J.L.; Cui, J.Z. On the microstructures, phase assemblages and properties of $Al_{0.5}CoCrCuFeNiSi_x$ high-entropy alloys. *J. Alloys Compd.* **2015**, *630*, 151–157. [CrossRef]
29. Wu, J.M.; Lin, S.J.; Yeh, J.W.; Chen, S.K.; Huang, Y.S.; Chen, H.C. Adhesive wear behavior of $Al_xCoCrCuFeNi$ high-entropy alloys as a function of aluminum content. *Wear* **2006**, *261*, 513–519. [CrossRef]
30. Li, M.Y.; Han, B.; Wang, Y.; Pu, K.J. Effects of La_2O_3 on the microstructure and property of laser cladding Ni-based ceramic coating. *Optik* **2017**, *130*, 1032–1037. [CrossRef]